Inorg. Chem. **2008**, *47*, 5267−5277

Manganese(II) Pyrimidine-4,6-dicarboxylates: Synthetic, Structural, Magnetic, and Adsorption Insights

Garikoitz Beobide,[†,‡] Wen-guo Wang,[§] Oscar Castillo,*[,†] Antonio Luque,[†] Pascual Román,[†] Giulia Tagliabue,[§,||] Simona Galli,*[,||] and Jorge A. R. Navarro*[,§]

Departamento de Química Inorgánica, Facultad de Ciencia y Tecnología, Universidad del País Vasco, Apartado 644, E-48080 Bilbao, Spain, Departamento de Procesos de Fabricación, Fundación Tekniker, Avda Otaola 20, E-20600 Eibar, Spain, Departamento de Química Inorgánica, Universidad de Granada, Avda Fuentenueva S/N, E-18071 Granada, Spain, and Dipartimento di Scienze Chimiche e Ambientali, Università dell'Insubria, Via Valleggio 11, I-22100 Como, Italy

Received February 15, 2008

A series of manganese(II) coordination polymers containing the bridging ligand pyrimidine-4,6-dicarboxylate (pmdc) have been prepared. The stoichiometries and structural features of these materials, which range from the one-dimensional (1D) chains in $\{[Mn(\mu\text{-pmdc})(H_2O)_3]\cdot 2H_2O\}_n$ (**1**) and $\{[Mn_2(\mu\text{-pmdc})_2(H_2O)_5]\cdot 2H_2O\}_n$ (**2**) to the two-dimensional layers in $\{[Mn(\mu_3\text{-pmdc})(H_2O)]\cdot H_2O\}_n$ (**3**) or the three-dimensional porous network in $\{[Mn(pmdc)]\cdot 2H_2O\}_n$ (**4**), are extremely dependent on the synthetic conditions (i.e., temperature and solvent). In spite of the structural diversity of these systems, crystallographic studies revealed that the pmdc ligand typically displays a tetradentate μ-(κO,κN:κO′′,κN′) coordination mode with the carboxylate groups almost coplanar with the pyrimidine ring [as in compounds **1** and **2** and compound **5** described below)]. In compound **3**, the pmdc moiety adopts a pentadentate μ_3-(κO,κN:κO′′,κN′:κO) coordination mode. The thermal, magnetic, and adsorption properties of these systems were also studied. The results showed that these compounds behave as antiferromagnets as a consequence of efficient magnetic exchange through the pmdc bridges. Compound **4** possesses permanent porosity, as proved by gas sorption data (N_2 at 77 K and CO_2 at 293 K). Finally, the heteronuclear iron(II)/manganese(II) compound $\{[FeMn(\mu\text{-pmdc})_2(H_2O)_5]\cdot 2H_2O\}_n$ (**5**), which is isomorphous to **2**, was also prepared and fully characterized.

Introduction

The study of structural and functional properties of coordination networks and polymers is one of the fastest-growing areas in the chemical and material sciences because of the wide variety of properties that these materials exhibit and the huge range of potential technological[1] and industrial[2] applications they present. The latter include storage of low-density fuel gases at safe pressures and room temperature,[3] gas mixture separations,[4] selective heterogeneous catalysis,[5] including some examples of regio-[6] and stereoselective processes,[7] and even controlled delivery of signal molecules

* To whom correspondence should be addressed. E-mail: oscar.castillo@ehu.es (O.C.), simona.galli@uninsubria.it (S.G.), jarn@ugr.es (J.A.R.N.).
† Universidad del País Vasco.
‡ Fundación Tekniker.
§ Universidad de Granada.
|| Università dell'Insubria.

(1) (a) Kepert, C. J. *Chem. Commun.* **2006**, 695. (b) Posch, D.; Ruiz-Molina, D.; Veciana, J. *Chem. Soc. Rev.* **2007**, *36*, 770. (c) Janiak, C. *Dalton Trans.* **2003**, 2781. (d) Kitagawa, S.; Kitaura, R.; Noro, S. *Angew. Chem., Int. Ed.* **2004**, *43*, 2334. (e) Robin, A. Y.; Fromm, K. M. *Coord. Chem. Rev.* **2006**, *250*, 2127.
(2) Mueller, U.; Schubert, M.; Teich, F.; Puetter, H.; Schierle-Arndt, K.; Pastre, J. *J. Mater. Chem.* **2006**, *16*, 626.
(3) Matsuda, R.; Kitaura, R.; Kitagawa, S.; Kubota, Y.; Belosludov, R. V.; Kobayashi, T. C.; Sakamoto, H.; Chiba, T.; Takata, M.; Kawazoe, Y.; Mita, Y. *Nature* **2005**, *436*, 238.
(4) (a) Pan, L.; Olson, D. H.; Ciemnolonski, L. R.; Heddy, R.; Li, J. *Angew. Chem., Int. Ed.* **2006**, *45*, 616. (b) Hayashi, H.; Cote, A. P.; Furukawa, H.; O'Keeffe, M.; Yaghi, O. M. *Nat. Mater.* **2007**, *6*, 501.
(5) Llabrés i Xamena, F. X.; Abad, A.; Corma, A.; García, H. *J. Catal.* **2007**, *250*, 294.
(6) Uemura, T.; Kitaura, R.; Ohta, Y.; Nagaoka, M.; Kitagawa, S. *Angew. Chem., Int. Ed.* **2006**, *45*, 4112.
(7) (a) Dybtsev, D. N.; Nuzhdin, A. L.; Chun, H.; Bryliakov, K. P.; Talsi, E. P.; Fedin, V. P.; Kim, K. *Angew. Chem., Int. Ed.* **2006**, *45*, 916. (b) Wu, C.-D.; Hu, A.; Zhang, L.; Lin, W. *J. Am. Chem. Soc.* **2005**, *127*, 8940.

10.1021/ic8002788 CCC: $40.75
Published on Web 05/21/2008

Scheme 1. Synthetic Routes and Conditions for Interconversions among Compounds **1**, **2**, **3**, and **4**

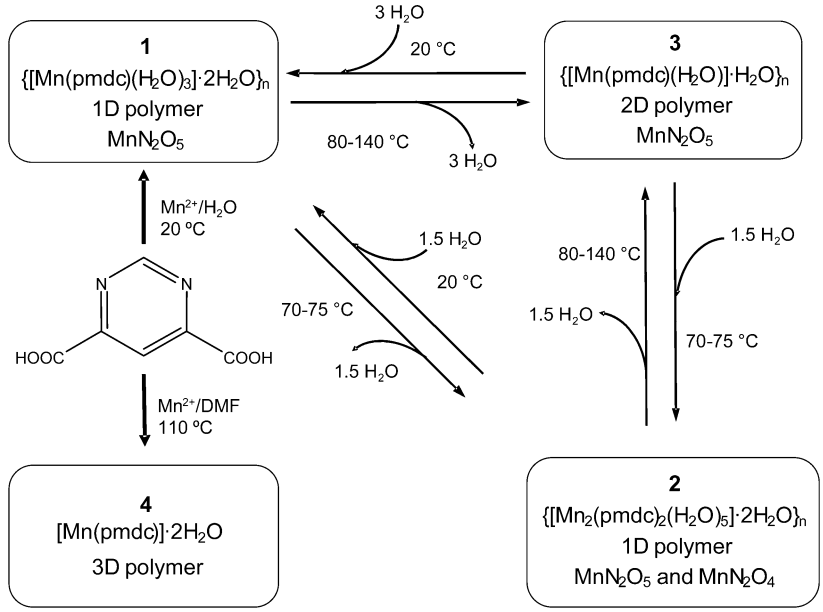

(e.g., NO) in biological applications.[8] In addition, coordination networks that exhibit bulk magnetism (e.g., hysteresis, spin-crossover, photomagnetism), photophysical or electrical properties, and second-harmonic generation have been prepared.[1]

We have previously shown that construction of extended coordination networks in a self-assembly process is facilitated by the use of simple, symmetric, nitrogen-containing heterocyclic ligands, which leads to the formation of materials possessing interesting functional aspects such as nonlinear optical,[9] magnetic,[10] thermal,[11] and adsorption properties.[12,13] It is noteworthy that the functionalities of these systems can be finely tuned through the coupling of appropriate metal ions and ligands. In this regard, we very recently reported a series of one-dimensional (1D) coordination polymers having the formula $\{[M(\mu\text{-pmdc})(H_2O)_2]\cdot H_2O\}_n$ (M = Fe, Co, Ni, Cu, Zn) that were obtained using a self-assembly process involving divalent first-row transition-metal ions and the symmetric ligand pyrimidine-4,6-dicarboxylate (pmdc), which typically adopted a tetradentate bischelate bridging mode.[14] Here we describe how the combination of this ligand with the coordination plasticity of the manganese(II) ion under various synthetic conditions (Scheme 1) yielded a variety of extended coordination compounds exhibiting structures ranging from the 1D chains in $\{[Mn(\mu\text{-pmdc})(H_2O)_3]\cdot 2H_2O\}_n$ (**1**), $\{[Mn_2(\mu\text{-pmdc})_2(H_2O)_5]\cdot 2H_2O\}_n$ (**2**), and $\{[FeMn(\mu\text{-pmdc})_2(H_2O)_5]\cdot 2H_2O\}_n$ (**5**) to the two-dimensional (2D) layers in $\{[Mn(\mu_3\text{-pmdc})(H_2O)]\cdot H_2O\}_n$ (**3**) or the three-dimensional (3D) porous network in $\{[Mn(pmdc)]\cdot 2H_2O\}_n$ (**4**). These systems were structurally characterized using single-crystal and powder X-ray crystallographic methods, and their thermal, magnetic, and adsorption properties were evaluated.

Experimental Section

Chemicals. All of the chemicals were of reagent grade and used as commercially obtained. The starting materials potassium hydrogen pyrimidine-4,6-dicarboxylate (KHpmdc) and pyrimidine-4,6-dicarboxylic acid (H_2pmdc) were prepared following the previously reported procedure.[15]

Synthesis of $\{[Mn(\mu\text{-pmdc})(H_2O)_3]\cdot 2H_2O\}_n$ (1). An aqueous solution (5 mL) of $Mn(NO_3)_2\cdot 4H_2O$ (0.0628 g, 0.25 mmol) was added dropwise to an aqueous solution (10 mL) of KHpmdc (0.0515 g, 0.25 mmol). The resulting light-yellow solution was allowed to evaporate at room temperature. Colorless single crystals of compound **1** were obtained after a few days. Yield: 80%. Anal. Calcd for $C_6H_{12}MnN_2O_9$ (**1**): C, 23.15; H, 3.89; N, 9.01; Mn, 17.66. Found: C, 23.20; H, 3.88; N, 9.10; Mn, 17.58. IR (KBr, cm^{-1}): 3464 (sh), 3367 (vs), ν(O−H); 3117 (w), ν(C−H); 1653 (vs), ν_{as}(O−C−O); 1600 (s), ν(C=C) + ν(C=N); 1471 (w), $\nu(C_{ar}-C)$; 1373 (vs), ν_s(O−C−O); 1311 (w), 1191 (w), 1093 (w), δ_{ip}(C−H); 1018 (w), δ_{op}(C−H); 928 (w), δ_{ring}; 729 (m), δ_{ip}(O−C−O); 698 (m), δ_{op}(O−C−O); 515 (w), τ_{ring}.

(8) Xiao, B.; Wheatley, P. S.; Zhao, X.; Fletcher, A. J.; Fox, S.; Rossi, A. G.; Megson, I. L.; Bordoga, S.; Regli, L.; Thomas, K. M.; Morris, R. E. *J. Am. Chem. Soc.* **2007**, *129*, 1203.
(9) Galli, S.; Masciocchi, N.; Cariati, E.; Sironi, A.; Barea, E.; Haj, M. A.; Navarro, J. A. R.; Salas, J. M. *Chem. Mater.* **2005**, *17*, 4815.
(10) (a) Beobide, G.; Castillo, O.; Luque, A.; García-Couceiro, U.; García-Terán, J. P.; Román, P. *Inorg. Chem.* **2006**, *45*, 5367. (b) Masciocchi, N.; Galli, S.; Sironi, A.; Galindo, M. A.; Barea, E.; Romero, M. A.; Salas, J. M.; Navarro, J. A. R.; Santoyo, F. *Inorg. Chem.* **2006**, *45*, 7612. (c) Navarro, J. A. R.; Barea, E.; Salas, J. M.; Masciocchi, N.; Galli, S.; Sironi, A. *Inorg. Chem.* **2007**, *46*, 2988.
(11) Masciocchi, N.; Ardizzoia, G. A.; LaMonica, G.; Maspero, A.; Sironi, A. *Eur. J. Inorg. Chem.* **2000**, 2507.
(12) (a) Tabares, L. C.; Navarro, J. A. R.; Salas, J. M. *J. Am. Chem. Soc.* **2001**, *123*, 283. (b) Barea, E.; Navarro, J. A. R.; Salas, J. M.; Masciocchi, N.; Galli, S.; Sironi, A. *Polyhedron* **2003**, *22*, 3051. (c) Barea, E.; Navarro, J. A. R.; Salas, J. M.; Masciocchi, N.; Galli, S.; Sironi, A. *J. Am. Chem. Soc.* **2004**, *126*, 3014. (d) Barea, E.; Navarro, J. A. R.; Salas, J. M.; Quirós, M. *Dalton Trans.* **2005**, 1743.
(13) (a) Navarro, J. A. R.; Barea, E.; Salas, J. M.; Masciocchi, N.; Galli, S.; Sironi, A.; Ania, C. O.; Parra, J. B. *Inorg. Chem.* **2006**, *45*, 2397. (b) Navarro, J. A. R.; Barea, E.; Salas, J. M.; Masciocchi, N.; Galli, S.; Sironi, A.; Ania, C. O.; Parra, J. B. *J. Mater. Chem.* **2007**, *17*, 1939. (c) Navarro, J. A. R.; Barea, E.; Rodríguez-Diéguez, A.; Salas, J. M.; Ania, C. O.; Parra, J. B.; Masciocchi, N.; Galli, S.; Sironi, A. *J. Am. Chem. Soc.* **2008**, *130*, 3978.
(14) Beobide, G.; Castillo, O.; Luque, A.; García-Couceiro, U.; García-Terán, J. P.; Román, P. *Dalton Trans.* **2007**, 2669.
(15) Hunt, R. R.; McOmie, J. F. W.; Sayer, E. R. *J. Chem. Soc.* **1959**, 525.

Table 1. Single-Crystal Data and Structure Refinement Details for Compounds **1**−**3** and **5**

	1	**2**	**5**	**3**
empirical formula	$C_6H_{12}MnN_2O_9$	$C_{12}H_{18}Mn_2N_4O_{15}$	$C_{12}H_{18}MnFeN_4O_{15}$	$C_6H_6MnN_2O_6$
formula weight	311.12	568.18	569.09	257.07
crystal system	monoclinic	triclinic	triclinic	orthorhombic
space group	$P2_1/c$	$P\bar{1}$	$P\bar{1}$	*Pbca*
a (Å)	12.204(5)	7.767(1)	7.7854(6)	9.971(1)
b (Å)	7.093(5)	10.281(2)	10.2442(8)	12.534(2)
c (Å)	14.846(4)	13.451(2)	13.395(1)	13.830(1)
α (deg)	90	100.18(1)	100.388(1)	90
β (deg)	121.96(2)	103.52(1)	103.293(1)	90
γ (deg)	90	103.82(1)	103.764(1)	90
V (Å^3)	1090.3(10)	982.9(3)	978.2(1)	1728.4(3)
Z	4	2	2	8
D_{obs} (g cm^{-3})	1.89(1)	1.91(1)	1.93(1)	1.97(1)
D_{calc} (g cm^{-3})	1.895	1.920	1.932	1.976
μ (mm^{-1})	1.258	1.375	1.477	1.540
R1[a]	0.0598	0.0412	0.0358	0.0321
wR2[b]	0.1355	0.0720	0.0897	0.0780

[a] $R1 = \sum||F_o| - |F_c||/\sum|F_o|$. [b] $wR2 = [\sum w(F_o^2 - F_c^2)^2/\sum w(F_o^2)^2]^{1/2}$.

Syntheses of {[Mn$_2$(μ-pmdc)$_2$(H$_2$O)$_5$]·2H$_2$O}$_n$ (2) and {[Mn(μ_3-pmdc)(H$_2$O)]·H$_2$O}$_n$ (3). Aqueous suspensions (15 mL) of compound **1** (0.0778 g, 0.25 mmol) were placed in a Teflon vessel surrounded by a steel casing, which was then placed on a heater. At temperatures above 50 °C, a mixture of crystals of compound **1** and **2** was obtained, whereas in the 70−75 °C range, only light-pink crystals of compound **2** were obtained (yield: 70%). Finally, in the temperature range 80−140 °C, yellow crystals of compound **3** were obtained (yield: 70%). Outside of these temperature ranges, mixtures of compounds were obtained.

Anal. Calcd for $C_{12}H_{18}MnN_4O_{15}$ (**2**): C, 25.35; H, 3.19; N, 9.86; Mn, 19.35. Found: C, 25.26; H, 3.29; N, 9.91; Mn, 19.24. IR (KBr, cm^{-1}): 3460 (vs), ν(O−H); 3113 (w), ν(C−H); 1648 (vs), ν_{as}(O−C−O); 1597 (s), 1536 (s), ν(C═C) + ν(C═N); 1373 (vs), ν_s(O−C−O); 1188 (w), 1093 (w), δ_{ip}(C−H); 1021 (w), δ_{op}(C−H); 927 (w), δ_{ring}; 727 (m), δ_{ip}(O−C−O); 700 (m), δ_{op}(O−C−O); 515 (w), τ_{ring}; 415 (w), ν(M−O) + ν(M−N).

Anal. Calcd for $C_6H_6MnN_2O_6$ (**3**): C, 28.02; H, 2.35; N, 10.90; Mn, 21.37. Found: C, 27.93; H, 2.24; N, 10.84; Mn, 21.37. IR (KBr, cm^{-1}): 3420 (vs), ν(O−H); 3120 (w), ν(C−H); 1671 (vs), 1636 (s), ν_{as}(O−C−O); 1604 (s), 1537 (m), ν(C═C) + ν(C═N); 1475 (w), ν(C$_{ar}$−C); 1364 (vs), ν_s(O−C−O); 1187 (w), 1107 (w), δ_{ip}(C−H); 1022 (w), δ_{op}(C−H); 924 (w), δ_{ring}; 742 (m), δ_{ip}(O−C−O); 693 (m), δ_{op}(O−C−O); 520 (w), τ_{ring}; 462 (w), ν(M−O) + ν(M−N).

Synthesis of [Mn(pmdc)(H$_2$O)$_3$]$_n$ (4). H$_2$pmdc (0.61 g, 3 mmol) was added to a solution of Mn(ClO$_4$)$_2$·6H$_2$O (1.45 g, 4 mmol) in DMF (25 mL). Heating the resulting suspension at 110 °C for 4 h with stirring yielded a yellow solid that was washed with DMF, ethanol, and diethyl ether. Yield: 90%. Anal. Calcd for $C_6H_8MnN_2O_7$ (**4**): C, 26.20; H, 2.93; N, 10.18; Mn, 19.97. Found: C, 26.37; H, 2.56; N, 10.21; Mn, 19.69. IR (KBr, cm^{-1}): 3425 (vs), ν(O−H); 1638 (vs), ν_{as}(O−C−O); 1594 (s), 1545 (s), ν(C═C) + ν(C═N); 1382 (vs), ν_s(O−C−O); 1193 (w), 1093 (w), δ_{ip}(C−H); 1025 (w), δ_{op}(C−H); 933 (w), δ_{ring}; 735 (m), δ_{ip}(O−C−O); 539 (w), τ_{ring}; 468 (w), ν(M−O) + ν(M−N).

Synthesis of {[FeMn(μ-pmdc)$_2$(H$_2$O)$_5$]·2H$_2$O}$_n$ (5). An aqueous solution (20 mL) containing H$_2$pmdc (2 mmol) and Fe(ClO$_4$)$_2$·6H$_2$O (0.25 g, 1 mmol) was heated at 90 °C for 1 h to produce a dark solution. After this solution was cooled, solid Mn(ClO$_4$)$_2$·6H$_2$O (0.36 g, 1 mmol) was added, forming a dark-red solution that yielded dark-red crystals suitable for X-ray diffraction after 1 month at room temperature. Yield: 70%. Anal. Calcd for $C_{12}H_{18}FeMnN_4O_{15}$ (**5**): C, 25.33; H, 3.19; N, 9.84; Mn, 9.65; Fe, 9.81. Found: C, 25.55; H, 3.19; N, 9.96; Mn, 9.63; Fe, 9.77. IR (KBr, cm^{-1}): 3406 (vs), ν(O−H); 1654 (vs), ν_{as}(O−C−O); 1599 (s), 1540 (s), ν(C═C) + ν(C═N); 1373 (vs), ν_s(O−C−O); 1189 (w), δ_{ip}(C−H); 1022 (w), δ_{op}(C−H); 927 (w), δ_{ring}; 728 (m), δ_{ip}(O−C−O); 696 (m), δ_{op}(O−C−O); 472 (w), ν(M−O) + ν(M−N).

Physical Measurements. Elemental analyses (C, H, N) were performed using a LECO CHNS-932 microanalytical analyzer. Metal content was determined using absorption spectrometry. IR spectra (KBr pellets) were recorded using a Mattson 1000 FTIR spectrometer over the 4000−400 cm^{-1} spectral region. Thermogravimetric (TG) and differential thermogravimetric (DTG) analyses as well as differential thermal analysis (DTA) were performed using a TA Instruments SDT 2960 thermal analyzer under a synthetic-air atmosphere (79% N$_2$/21% O$_2$) with a heating rate of 5 °C min^{-1}. Magnetic measurements were performed on polycrystalline samples of the compounds using a Quantum Design SQUID susceptometer covering the temperature range 2.0−300 K at 0.5 T. The susceptibility data were corrected for diamagnetism (estimated from Pascal's tables[16]), temperature-independent paramagnetism, and magnetization of the sample holder. Sorption isotherms were measured using a Micromeritics Tristar 3000 volumetric instrument under continuous adsorption conditions. Prior to measurement, powder samples were heated at 130 °C for 2 h and outgassed to 10^{-3} Torr using a Micromeritics Flowprep degasser. Brunauer−Emmet−Teller (BET) and Langmuir analyses were used to determine the total specific surface areas for the N$_2$ isotherms.

Single-Crystal X-ray Data Collection and Structure Determination. Data collections on single crystals of compounds **1**−**3** and **5** were carried out at 293 K using an Xcalibur diffractometer equipped with an area detector and graphite-monochromatized Mo Kα radiation (λ = 0.71073 Å). The data reduction was performed using the CrysAlis RED program.[17] Information concerning the data collection is summarized in Table 1. The structures were solved using direct methods with the SIR97 program.[18] Full-matrix least-squares refinements on F^2 were performed using SHELXL97.[19] All of the non-hydrogen atoms were refined anisotropically. The hydrogen atoms of the pyrimidine ring were positioned geo-

(16) Earnshaw, A. *Introduction to Magnetochemistry*; Academic Press: London, 1968.
(17) *CrysAlis RED*, version 1.170; Oxford Diffraction: Wroclaw, Poland, 2003.
(18) Altomare, A.; Burla, M. C.; Camalli, M.; Cascarano, G. L.; Giacovazzo, C.; Guagliardi, A.; Moliterni, A. G. G.; Spagna, R. *J. Appl. Crystallogr.* **1999**, *32*, 115.
(19) Sheldrick, G. M. *SHELXS97 and SHELXL97*; University of Göttingen: Göttingen, Germany, 1997.

Table 2. Selected Bond Lengths (Å) in Compounds **1**−**3** and **5**[a]

1		**2**		**5**		**3**	
Mn1−N1	2.351(2)	Mn1−N11	2.337(2)	Fe1−N11	2.269(2)	Mn1−N1	2.323(2)
Mn1−O81	2.196(2)	Mn1−N21	2.288(2)	Fe1−N21	2.228(2)	Mn1−O81	2.093(1)
Mn1−N3a	2.506(2)	Mn1−O2w	2.167(2)	Fe1−O2w	2.162(2)	Mn1−N3a	2.302(1)
Mn1−O71a	2.186(2)	Mn1−O1w	2.108(2)	Fe1−O1w	2.078(2)	Mn1−O71a	2.177(1)
Mn1−O1w	2.294(2)	Mn1−O181	2.129(2)	Fe1−O181	2.080(2)	Mn1−O71b	2.184(1)
Mn1−O2w	2.193(2)	Mn1−O281	2.160(2)	Fe1−O281	2.112(2)	Mn1−O1w	2.151(1)
Mn1−O3w	2.290(2)	Mn2−N13a	2.405(2)	Mn2−N13a	2.401(2)		
		Mn2−N23	2.433(2)	Mn2−N23	2.435(2)		
		Mn2−O171a	2.204(2)	Mn2−O171a	2.198(2)		
		Mn2−O271	2.203(1)	Mn2−O271	2.199(2)		
		Mn2−O3w	2.241(2)	Mn2−O3w	2.255(2)		
		Mn2−O4w	2.245(2)	Mn2−O4w	2.251(2)		
		Mn2−O5w	2.197(2)	Mn2−O5w	2.209(2)		

[a] Symmetry codes: for **1**, (a) $-x, y - {}^1/_2, -z - {}^3/_2$; for **2** and **5**, (a) $x + 1, y, z$; for **3**, (a) ${}^1/_2 + x, {}^1/_2 - y, 1 - z$ and (b) $-{}^1/_2 - x, -{}^1/_2 + y, z$.

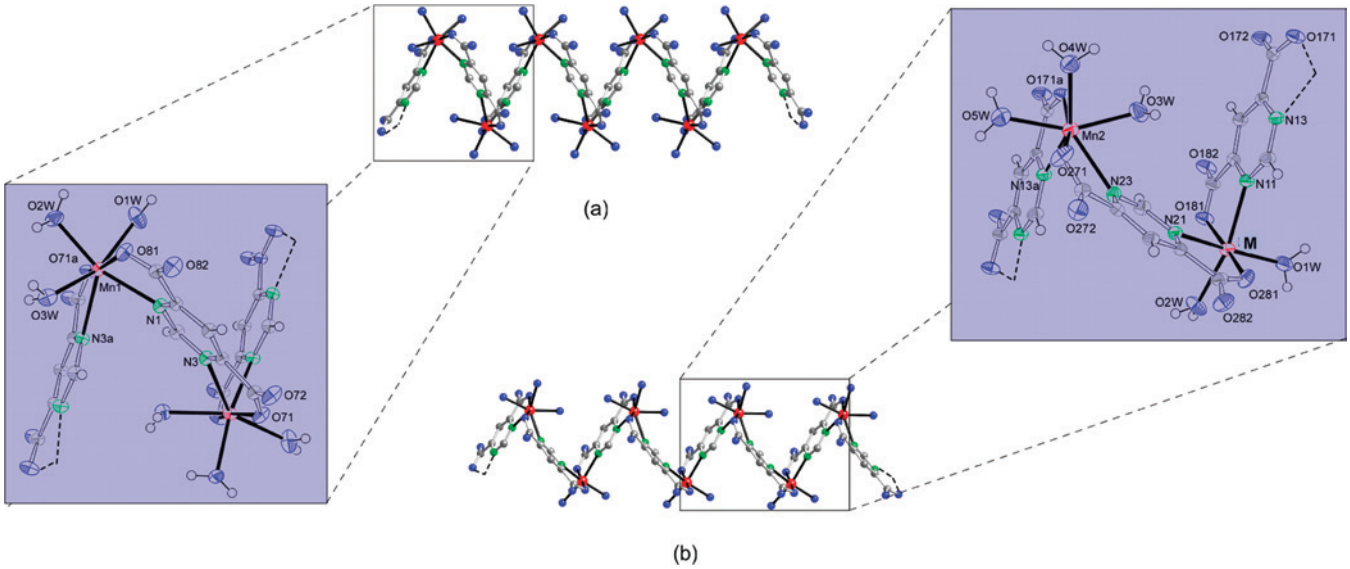

Figure 1. Perspective drawings of fragments of the 1D chains in (a) compound **1** and (b) compounds **2** and **5**. The expanded views (shaded) show ORTEP graphics of the M(II) coordination environments and the labeling schemes used.

metrically and allowed to ride on their parent atoms with $U_{iso} = 1.2U_{iso}$(parent). Water hydrogen atoms were located using a Fourier difference map and introduced as fixed contributors with $U_{iso} = 1.5U_{iso}$(parent). All of the calculations were performed using the WinGX crystallographic software package.[20]

Results and Discussion

Structural Description. A structural feature common to compounds **1**, **2**, and **5** and encountered even in the previously characterized materials $\{[M(\mu\text{-pmdc})(H_2O)_2]\cdot H_2O\}_n$ (M = Fe, Co, Ni, Cu, Zn)[14] is the tetradentate μ-(κO,κN:κO′′,κN′) coordination mode of the pyrimidine-4,6-dicarboxylate anion. Notably, species **3** constitutes an exception, in that the pmdc moiety adopts a pentadentate μ_3-(κO,κN:κO′′,κN′:κO) coordination type. Despite the almost exclusive recurrence of a single ligand coordination mode, the great coordination flexibility of manganese(II), which is tuned by means of temperature-directed entropic and solvent effects, resulted in the isolation of different architectures based on the same [M(pmdc)] building block. Thus, as later described, the crystal structures of compounds **1**, **2**, and **5** consist of $\{[M(\mu\text{-pmdc})]\}_n$ corrugated chains in which the additional M(II) coordination sites are occupied by water molecules. In contrast, the skeleton of the more compact species **3** can be rationalized as the fusion of corrugated parallel chains through already-bound carboxylate oxygen atoms, which replace two of the coordinated water molecules in **1**, **2**, and **5**.

Structural details and selected bond lengths for compounds **1**−**3** and **5** are provided in Tables 1 and 2, respectively.

$\{[Mn(\mu\text{-pmdc})(H_2O)_3]\cdot 2H_2O\}_n$ (1), $\{[Mn_2(\mu\text{-pmdc})_2(H_2O)_5]\cdot 2H_2O\}_n$ (2), and $\{[FeMn(\mu\text{-pmdc})_2(H_2O)_5]\cdot 2H_2O\}_n$ (5). Compound **1** crystallizes in the monoclinic $P2_1/c$ space group, while the isomorphous species **2** and **5** are triclinic with space group $P\bar{1}$. As anticipated, the three compounds contain 1D zigzag polymeric chains built upon consecutive [M(pmdc)] (M = Mn, Fe) monomers. The coordination about the metal centers, the labeling schemes, and fragments of the polymeric chains are shown in Figure 1. The pmdc ligands adopt a μ-(κO,κN:κO′′,κN′) coordination mode, and their N,O chelation results in the formation of two five-membered chelate rings for each metal ion. The remaining M(II) coordination sites are occupied by water molecules. In spite of this, some structural differences exist,

(20) Farrugia, L. J. *WINGX: A Windows Program for Crystal Structure Analysis*; University of Glasgow: Glasgow, U.K., 1998.

which can be mainly traced back to (i) the number of coordinated water molecules (three in **1** and two and three alternately in **2** and **5**) and (ii) the metal content [Mn in **1** and **2** and mixed Fe/Mn (1:1) in **5**]. Indeed, in **1**, the unique, crystallographically independent Mn(II) ion is bound to three water molecules in a *mer*-$[Mn(H_2O)_3]^{2+}$ fashion; the further assistance of two nitrogen and two oxygen atoms from two pmdc ligands implies an overall coordination sphere of the MnN_2O_5 type, resembling a monocapped octahedron, with one bond (Mn1−N3a) significantly longer than the other ones (Table 2). On the contrary, in **2** and **5**, *cis*-$[M(H_2O)_2]^{2+}$ (M = Mn in **2**, Fe in **5**) and *mer*-$[Mn(H_2O)_3]^{2+}$ units alternate along the $\{[M(\mu\text{-pmdc})]\}_n$ chains.

Within the *cis*-$[M(H_2O)_2]^{2+}$ units in **2** and **5**, the M(II) ions exhibit octahedral MN_2O_4 stereochemistry completed by O and N atoms from two crystallographically independent ligands (pmdc1 and pmdc2 in the following discussion). As in compound **1**, the Mn(II) centers in the *mer*-$[Mn(H_2O)_3]^{2+}$ units of **2** display monocapped octahedral MN_2O_5 stereochemistry, with two coordination distances significantly longer than the others (Table 2). Notably, in the heteronuclear compound **5**, the Fe(II) and Mn(II) metal centers are not statistically distributed along the 1D chains, yet they alternate in an ordered manner. Thus, the Mn(II) ions are exclusively heptacoordinate and have virtually the same metal-to-ligand distances and angles as the heptacoordinate Mn(II) ions in **2**. The Fe(II) ions adopt the octahedral environment but have slightly shorter (0.05 Å) metal-to-ligand distances than the octahedral Mn(II) ions in **2**, in agreement with its smaller ionic radius [0.75 vs 0.81 Å for hexacoordinate high-spin Fe(II) and Mn(II), respectively].[21] Notably, the different preferences for heptahedral coordination environments found for the divalent iron and manganese cations was supported by a search of the Cambridge Structural Database,[22] which retrieved 61 heptacoordinate metal complexes of Mn^{2+} but only 18 of Fe^{2+}.

As expected, the different crowding around the metal centers induce (i) significantly longer bond lengths around the heptacoordinate ions [mean Mn−N distances of 2.428 Å in **1** and 2.419 Å in **2** and mean Mn−O distances of 2.232 Å in **1** and 2.225 Å in **2**] than around the hexacoordinate ones [mean M−N and M−O distances of 2.318 and 2.144 Å, respectively, in **2**]; (ii) a more acute M···M···M angle in compound **1** (63.2°) than in compounds **2** and **5** (71.2° in **2**); (iii) a wider N−Mn−O bite angle for the hexacoordinate Mn(II) ions than for the heptacoordinate ones (e.g., average values of 73.4 vs 69.9°, respectively, are found in **2**); and (iv) a significantly wider dihedral angle between the mean planes of the two ligands chelating a given metal center in **2** and **5** (e.g., 74.14° in **2**) than in **1** (58.18°).

The bridged M···M distances are 6.767(1) Å in compound **1**, while they are 6.765(1) and 6.575(1) Å in compound **2** and 6.705(1) and 6.521(1) Å in compound **5** for ligands pmdc1 and pmdc2, respectively.

In compound **1**, the pmdc ligand is essentially planar, with the carboxylate groups rotated slightly (5.9°) out of the pyrimidine plane; the ligands in compound **2** exhibit somewhat more nonplanarity, with dihedral angles of up to 16.2° for pmdc2.

In compound **1**, the chains run along the crystallographic *b* axis in such a way that each one interacts with four other surrounding chains by means of an intricate hydrogen-bonding network (see Table S1 in the Supporting Information). Altogether, hydrogen-bonding interactions are present between both coordinated and lattice water molecules and the swinging oxygen atoms of the carboxylate groups (Figure 2a). Notably, one of the water molecules of crystallization (O4w) is located in the void generated among four interconnected chains, while the second one (O5w) is deeply buried in the chain folds.

In compounds **2** and **5**, the chains run along the crystallographic *a* axis (Figure 2b), and their reciprocal dispositions show a great resemblance to that of **1**. Nonetheless, the smaller number of water molecules per metal ion allows closer packing in which every chain is directly hydrogen-bonded to six surrounding ones. The water molecules of crystallization (O6w and O7w) are exclusively located within the folds of the chains, and they establish hydrogen-bonding interactions with the host chain and a neighboring one.

$\{[Mn(\mu_3\text{-pmdc})(H_2O)]\cdot H_2O\}_n$ (3). Single-crystal X-ray analysis showed that compound **3** crystallizes in the orthorhombic *Pbca* space group and consists of 2D layers having the formula $\{[Mn(\mu_3\text{-pmdc})(H_2O)]\}_n$ surrounded by water molecules of crystallization. The Mn(II) ions exhibit distorted octahedral stereochemistry (Figure 3) of the MnN_2O_4 type completed by two pyrimidine nitrogen atoms and three carboxylate oxygen atoms from three symmetry-related pmdc ligands and the oxygen atom of one water molecule. Thus, in contrast to what is found in compounds **1** and **2**, each pmdc ligand in **3** globally bridges three Mn(II) ions, adopting a pentadentate μ_3-($\kappa O\kappa N$:$\kappa O''$,$\kappa N'$:κO) coordination mode. The N,O chelation results in the formation of two five-membered chelate rings (with bite angles of 74.85 and 72.52°) for each Mn(II) ion. The shortest M···M distances within the two-dimensional coordination network are 3.487 Å along the bis(μ-oxo) bridge and 6.664 Å through the μ-pyrimidine bridge. The pmdc ligand deviates slightly from planarity, with dihedral angles of 3.3 and 9.4° between the pyrimidine ring and the carboxylate groups.

The coordination network can be viewed as the fusion of polymeric 1D $\{[Mn(\mu\text{-pmdc})(H_2O)]\}_n$ zigzag chains by means of Mn−O bonds involving already-coordinated oxygen atoms (O71) of pmdc ligands belonging to adjacent chains, which replace the coordinated water molecules released in going from **1** or **2** to **3**. Therefore, the dimensionality of the coordination connectivity is increased to yield an overall 2D folded skeleton containing oblong cavities (Figure 4) having dimensions of 3.6 × 6.8 Å (estimated by subtraction of the pertinent van der Waals radii); these cavities are large enough to host two symmetry-related O1w water molecules. These molecules interact with the coordinated water molecule and the swinging oxygen atom of a neighboring carboxylate group through hydrogen bonds,

(21) Shannon, R. D. *Acta Crystallogr.* **1976**, *A32*, 751.
(22) Allen, F. H. *Acta Crystallogr.* **2002**, *B58*, 380.

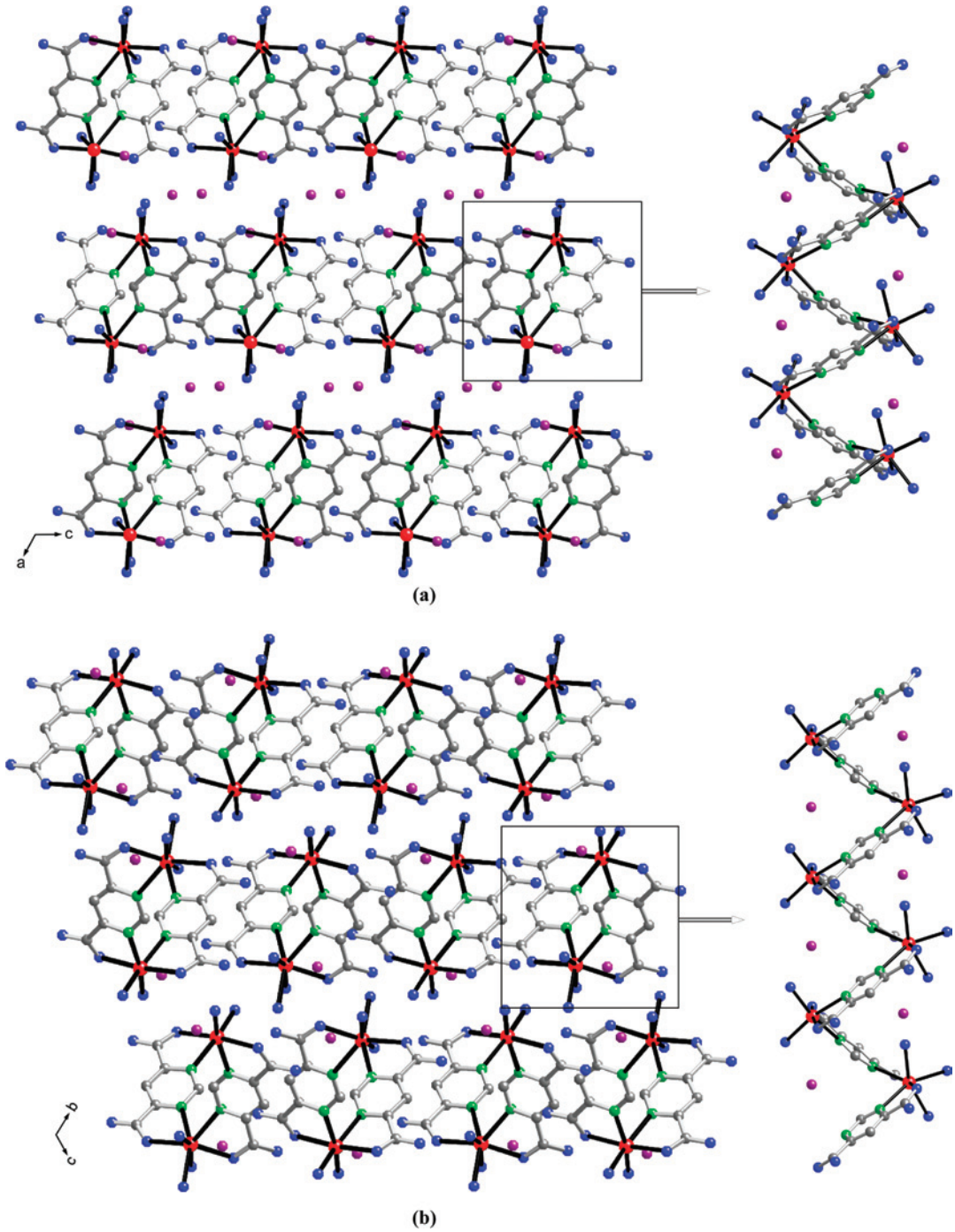

Figure 2. (left) Views of the crystal packing of (a) compound **1** along the [010] direction and (b) compound **2** along [100]. (right) Water molecules of crystallization inserted in the folds of the 1D chains in both compounds. Color code: carbon (gray), nitrogen (green), oxygen atoms of carboxylate groups and coordinated water molecules (blue), and water molecules of crystallization (pink). Hydrogen atoms have been omitted for clarity.

thereby connecting consecutive layers and creating a 3D network. Because of the symmetry requirements of the crystallographic *a* glide plane, isolated cavities rather than channels are formed (Figure 5), thus preventing easy release of the water molecules and adsorption of guest molecules. Accordingly, TG measurements indicated loss of water only above 170 °C (see Figure S1 in the Supporting Information).

Mutual Interconversion of 1, 2, and 3. At this point, it is worth emphasizing some remarkable aspects of the synthesis of these compounds. The first of these concerns the effect of the synthetic conditions, specifically temperature and pressure, on the resulting crystal structure. Increasing the temperature leads to retention of a smaller number of water molecules in the lattice and therefore to an increase in the entropy of the system (due to the greater conformational freedom of the released water molecules). One consequence correlated with the release of water is the more effective packing of the resulting structure, as evidenced by the increase in the density values in going from **1** to **3** [1.895, 1.920, and 1.976 g cm^{-3}, respectively (Table 1)] and the self-assembly of the 1D polymeric chains seen in **1** and **2** to yield the overall 2D covalent framework in **3** under soft

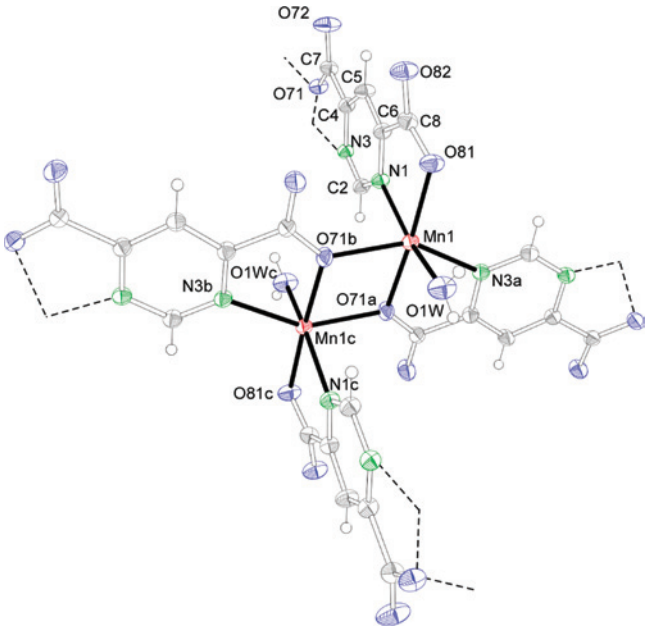

Figure 3. ORTEP view of the Mn(II) coordination environment in compound **3**. The labeling scheme is also shown.

hydrothermal conditions. Indeed, it is well-known that hydrothermal synthesis is an effective and powerful tool for the construction of high-dimensionality metal−organic frameworks.[23] Under these synthetic conditions, it is more probably the metastable kinetic phases that are isolated rather than the thermodynamically stable ones;[24] therefore, when compound **3** is suspended in an aqueous solution and stirred for 48 h at ambient conditions, interconversion to the thermodynamically stable compound **1** occurs.

The easy interconversion of compounds **1**−**3** is also worthy of mention. Each of them can be obtained from either of the other two by subjecting an aqueous suspension of the crushed starting material to the appropriate synthetic conditions detailed in Scheme 1. The presence of well-shaped crystals in the resulting product in all cases possibly indicates that the interconversion process takes places through a solubilization/crystallization process. Moreover, as confirmed by thermodiffractometric studies (Figure 6), the similarity of the crystal structures of compounds **1** and **2** allows the solid-state transformation of **1** into **2** at 40 °C with retention of crystallinity, which is a nice example of a topic recently investigated in the literature.[25] At temperatures above 70 °C, a subsequent dehydration process leads to a poorly crystalline phase whose diffractogram does not bear any resemblance to those of the reported compounds. In contrast, compound **4** is not involved in these kinds of transformations. Its structure does not change upon release of water molecules, and it reversibly adsorbs moisture from the environment after heating. On the other hand, samples of compound **2** under room conditions slowly evolve into compound **1**, while compounds **3** and **4** are more stable in air and show no evidence of crystal decomposition.

Comments on the Crystal Structure of Compound 4. Compound **4** possesses a clear stoichiometry, which we derived from thermogravimetric and elemental analyses. Its X-ray powder diffraction (XRPD) pattern (Figure 7) shows that it is a very crystalline material that can be described by a bcc lattice having $a = 18.67$ Å and $V = 6507.8$ Å^3 (based on a Le Bail refinement with the following pertinent figures of merit: Rwp = 0.084 and Rp = 0.060). No extinctions other than $h + k + l = 2n + 1$ could be observed, indicating that many space groups are equally good candidates. Density considerations [$D_{obs} = 1.65(2)$ g cm^{-3}, measured by flotation of a pressed disk of the powdered compound] lead to an estimated Z value of 24 [$D_{calc} = 1.68$ g cm^{-3}]. However, no structural model could be built using either conventional reciprocal-space techniques or simulated-annealing direct-space methods. While the former are known to fail for low-symmetry Laue classes (indicating 'exact' overlap of non-equivalent reflections), the failure to find a solution using direct-space techniques was more surprising but still understandable: indeed, conventional intensity-extraction methods use equipartitioning of overlapping reflections. Apparently, in nonholoedric Laue groups, this problem has not yet found appropiate solution.[26] We used different sample sizes and preparation modes and repeatedly checked the reproducibility of the XRPD acquisitions, thereby confirming the absence of a preferred orientation and hydration/dehydration effects, yet we did not succeed in solving the structure. However, during the manuscript review process, we found a report[27] of a sodalitic species having the formula $[In(C_6N_2O_4H_2)_2Na_{0.36}K_{1.28}](NO_3)_{0.64}(H_2O)_{2.1}$ and possessing a unit cell and crystallographic symmetry closely related to those of **4**. A preliminary structure solution based on structural information for the In(III) compound has been carried out and confirms that **4** is also a sodalitic porous material containing large cavities (which are hydrated in air at room temperature), as found for the species M(X-pymo)$_2$ (M = Cu, Pd; X-pymo = 5-X-pyrimidin-2-olate, X = H, F).[12a,c,13]

Electronic and Magnetic Properties. As expected, the electronic spectra of compounds **1**−**4** did not show any crystal-field d−d transitions; only intraligand $\pi-\pi$ transitions centered at 38 500 cm^{-1} appeared. In contrast, the incorporation of Fe(II) ions in **5** resulted in the appearance of strong band at 18900 cm^{-1} that was attributed to a possible intervalence transition between Fe and Mn as well as a d−d absorption band centered at 9700 cm^{-1} that is typical of high-spin Fe(II).[28]

Compounds **1**−**3** showed room-temperature $\chi_M T$ values (Table 3) close to that expected for an uncoupled manganese(II) ion ($g = 2.0$, $\chi_M T = 4.38$ cm^3 K mol^{-1}). In the case of **5**, the $\chi_M T$ value fell between those expected for manganese(II) and high-spin iron(II). In all cases, the $\chi_M T$ value decreased gradually as the sample was cooled (Figure 8), indicating an overall antiferromagnetic behavior. In

(23) Cheetham, A. K.; Rao, C. N. R.; Feller, R. K. *Chem. Commun.* **2006**, 4780.
(24) Hagrman, P. J.; Finn, R. C.; Zubieta, J. *Solid State Sci.* **2001**, *3*, 745.
(25) Habib, H. A.; Sanchiz, J.; Janiak, C. *Dalton Trans.* **2008**, 1734.
(26) Altomare, A. Istituto di Cristallografia, Sede di Bari, Bari, Italy. Personal communication, 2008.
(27) Sava, D. F.; Kravtsov, V.; Nouar, F.; Wojtas, L.; Eubank, J. F.; Eddaoudi, M. *J. Am. Chem. Soc.* **2008**, *130*, 3768.
(28) Garner, M.; Lewinski, K.; Pattek-Janczyk, A.; Reglinski, J.; Sieklucka, B.; Spicer, M. D.; Szaleniec, M. *Dalton Trans.* **2003**, 1181.

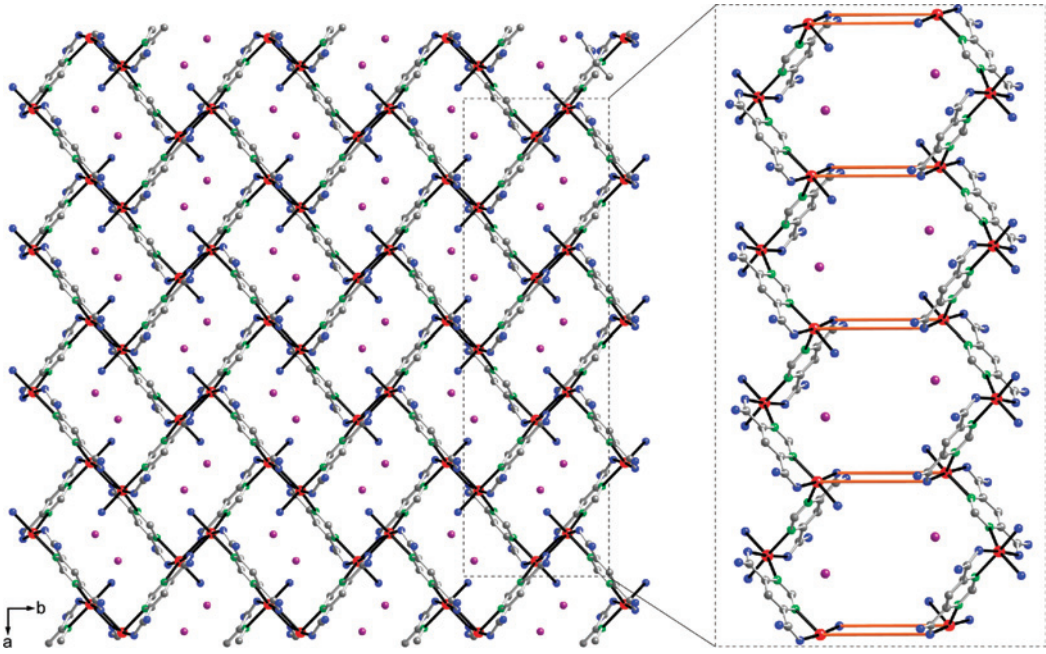

Figure 4. Views of the structure of compound **3**: (left) the 2D skeleton; (right) the μ-oxo bridges (in red) between the chains.

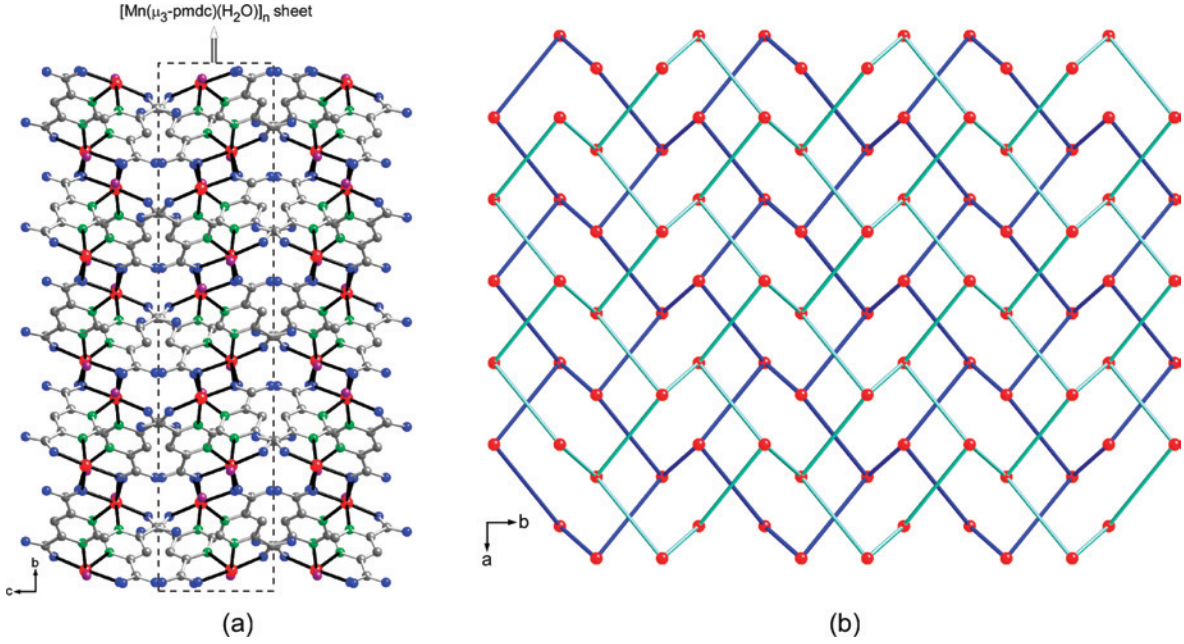

Figure 5. (a) View of compound **3** along the [100] direction. (b) Schematic view of the stacking of the sheets along the [001] direction. The upper and lower sheets are represented in different colors.

addition, the absence of maximums in the χ_M curves suggested the presence of weak magnetic interactions. This behavior agrees with the observations of antiferromagnetic interactions reported for metal ions containing unpaired e_g electrons and bridged by pyrimidine type-ligands,[13,29] in contrast with the ferromagnetic behavior usually observed for compounds containing only unpaired t_{2g} electrons.[30]

In view of the molecular structures of compounds **1** and **2**, their magnetic data were fitted using the classical Heisenberg spin model for a regular antiferromagnetic chain ($\hat{H} = -J\sum_i \hat{\mathbf{S}}_i \cdot \hat{\mathbf{S}}_{i+1}$)[31] with $S = {}^5/_2$. It is deserving of note that the magnetic interactions between the paramagnetic centers in these complexes take place mainly through the pyrimidine ring, since for a bis(bidentate) pmdc bridge, the contribution from the carboxylato groups can be considered negligible because of the long magnetic pathway involving

(29) (a) Ishida, T.; Kawakami, T.; Mitsubori, S.-i.; Nogami, T.; Yamaguchi, K.; Iwamura, H. *J. Chem. Soc., Dalton Trans.* **2002**, 3177. (b) Ezhura, T.; Endo, K.; Matsuda, K.; Aoyama, Y. *New J. Chem.* **2000**, *24*, 609. (c) Manson, J. L.; Gu, J.; Schlueter, J. A.; Wang, H. H. *Inorg. Chem.* **2003**, *42*, 3950. (d) Yasui, M.; Ishikawa, Y.; Akiyama, N.; Ishida, T.; Nogami, T.; Iwasaki, F. *Acta Crystallogr.* **2001**, *B57*, 288.

(30) (a) Ishida, T.; Mitsubori, S.; Nogami, T.; Takeda, N.; Ishikawa, M.; Iwamura, H. *Inorg. Chem.* **2001**, *40*, 7059. (b) Mohri, F.; Yoshizawa, K.; Yamabe, T.; Ishida, T.; Nogami, T. *Mol. Eng.* **1999**, *8*, 357.

(31) Fisher, M. E. *Am. J. Phys.* **1964**, *32*, 343.

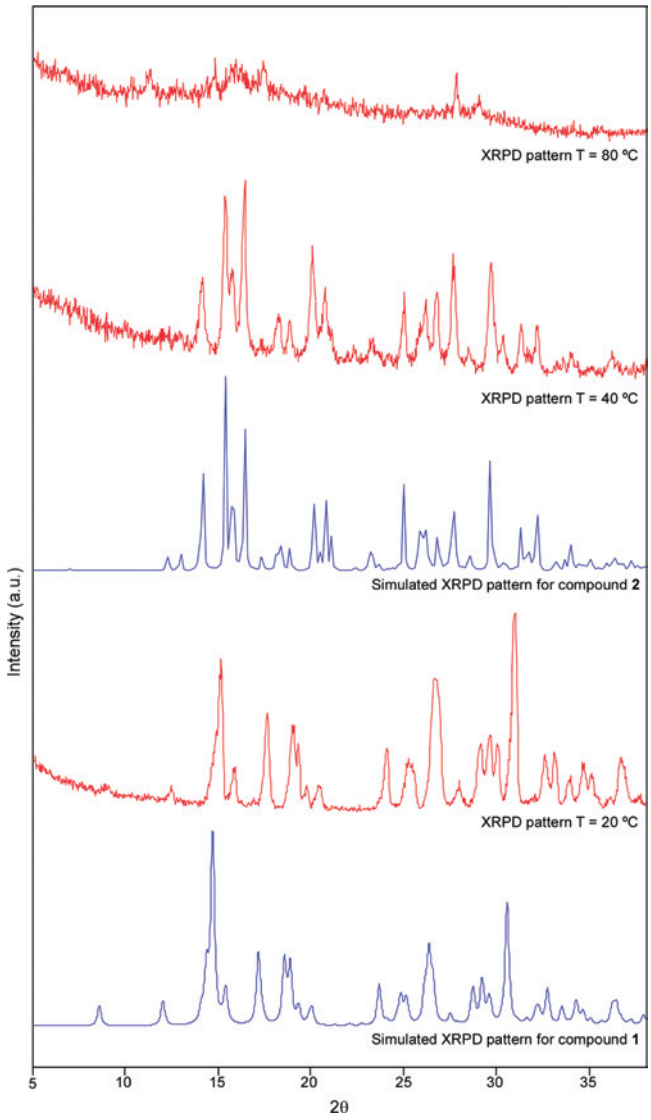

Figure 6. Selected XRPD patterns (red traces) obtained during thermal treatment of compound **1**. For comparison, simulated XRPD patterns for **1** and **2** (blue traces) are also shown.

these groups.[14,32] In fact, the J values obtained for compounds **1** and **2** agree fairly well with previously reported magnetic data for pyrimidine-bridged Mn(II) complexes (J values ranging from -0.2 to -0.3 cm^{-1}).[29a,33]

The regular alternation of high-spin Fe^{2+} (d^6) and Mn^{2+} (d^5) ions along the chains in compound **5** could have lead to ferrimagnetic behavior at low temperatures if the magnetic interaction through the pmdc bridges had been strong enough. In the present case, however, the minimum on the $\chi_M T$ curve typical of a ferrimagnetic compound was not observed. This fact was attributed to the weakness of the magnetic interactions; indeed, the $\chi_M T$ value at 2 K was 1.33 cm^3 K mol^{-1}, which is much greater than the theoretical value of 0.87 cm^3 K mol^{-1} for 0.5 unpaired electrons per metal center. In order to estimate the value of the magnetic coupling in **5**, the magnetic data for this compound were fitted to the analytical expression derived by Drillon et al.[34] for alternating chains of classical spins; this procedure yielded a J value of -0.38 cm^{-1}.

The complex connectivity among the metal centers in compound **3** and the preliminary results on the crystal structure of compound **4** precluded a quantitative estimation of the coupling constant. Therefore, in order to perform a comparative study of the efficiency of the pmdc bridges in transmitting the magnetic interaction, the susceptibility data were satisfactorily fit to the Curie−Weiss equation: $\chi_M = C/(T - \theta)$, where $C = Ng^2\mu^2S(S + 1)/3k$]. The C and θ values obtained from this fit (Table 3) are characteristic of weak antiferromagnetic coupling of the metal centers transmitted through the pmdc bridges and indicate a slightly stronger interaction in compound **3** than in compounds **1** and **2** (as evidenced by the θ values), in good agreement with the greater connectivity among the metal centers in **3**. The results show that these interactions are weaker than those found in the Fe−Cu series,[14] which should be related to the increasing numbers of $t_{2g}-t_{2g}$ and $t_{2g}-e_g$ ferromagnetic terms along the series.

Adsorption Properties. The gas-adsorption performances of solids **1**, **2**, **3**, and **4** toward N_2 and CO_2 were studied in order to determine the textural properties of these compounds and their potential for use in gas separation and storage applications. The results show that **1**−**3** do not adsorb the tested gases but **4** behaves as a microporous material.

The adsorption isotherm of **4** toward N_2 (Figure 9a) possesses a type-I−IV hybrid shape with a (type H1) hysteresis loop at relative pressures greater than 0.8, which can be attributed to textural mesoporosity arising from interparticle mesopores. The isotherm also exhibits a sharp knee at low relative pressures ($p/p^\circ < 0.01$) followed by a plateau corresponding to filling of the microporous structure, indicating that the permanent porosity of the sample is mainly composed of micropores of rather uniform size, consistent with the preliminary crystallographic data (see above). The low onset pressure and the sharp rise of the isotherm indicate that a deep potential well forms in the micropores. Fitting the isotherm to the Langmuir equation in the low-pressure region ($p/p^0 < 0.2$) gave a very large value of 410 m^2 g^{-1} for the specific surface area.

The CO_2 adsorption measurements also indicate that **4** possesses permanent porosity in the microporous region, which is manifested by the steep slope of the type-I isotherm at low relative pressures (see Figure 9b). The amount of CO_2 adsorbed (40 cm^3 g^{-1}) at 293 K and 650 torr was very high. This high storage capacity at room temperature should indicate that the porous network is fully accessibile to the adsorbate molecules and that, as previously mentioned, a deep potential well forms in the pores. The adsorption performance of **4** toward CO_2 clearly approaches the values found for the best porous pyridimine derivatives, being surpassed only by that for [Pd(X-pyrimidin-2-olate)$_2$]$_n$ (X = H, F) sodalitic frameworks,[13] and should be taken as

(32) Beobide, G.; Castillo, O.; García-Couceiro, U.; García-Terán, J. P.; Luque, A.; Martínez-Ripoll, M.; Román, P. *Eur. J. Inorg. Chem.* **2005**, 2586.

(33) (a) Lloret, F.; Julve, M.; Cano, J.; De Munno, G. *Mol. Cryst. Liq. Cryst.* **1999**, *334*, 569. (b) Escuer, A.; Vicente, R.; Mautner, F. A.; Goher, M. A. S.; Abu-Youssef, M. A. M. *Chem. Commun.* **2002**, 64.

(34) Drillon, M.; Coronado, E.; Beltran, D.; Georges, R. *Chem. Phys.* **1983**, *79*, 449.

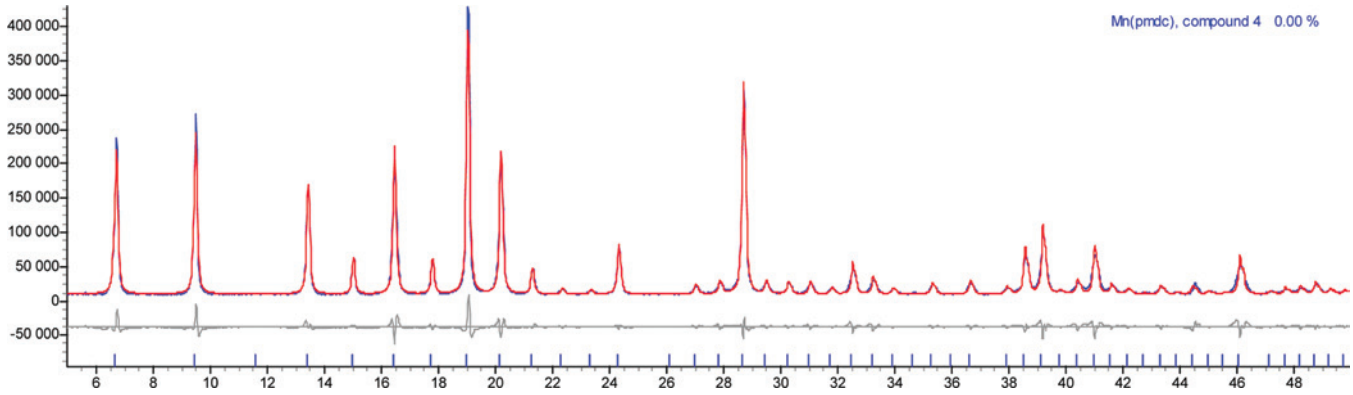

Figure 7. Le Bail refinement of compound **4** in terms of experimental (blue), calculated (red), and difference (grey) XRPD profiles. Peak markers are shown at the bottom. Horizontal axis: 2θ (deg); vertical axis: counts.

Table 3. Best-Fit Values of Magnetic Properties for Compounds **1**−**5**

compound	$\chi_M T$ at 300 K (cm^3 K mol^{-1})	J (cm^{-1})	g	C (cm^3 K mol^{-1})	θ (K)
1[a]	4.28	−0.18	2.00	4.30	−1.9
2[a]	4.38	−0.22	2.00	4.40	−1.7
3	4.51	–	–	4.53	−2.4
4	3.89	–	–	3.92	−1.5
5[b]	3.87	−0.38	2.00(Mn)/2.18(Fe)	3.92	−2.5

[a] 1D Heisenberg model. [b] 1D alternating chain of classical spins.

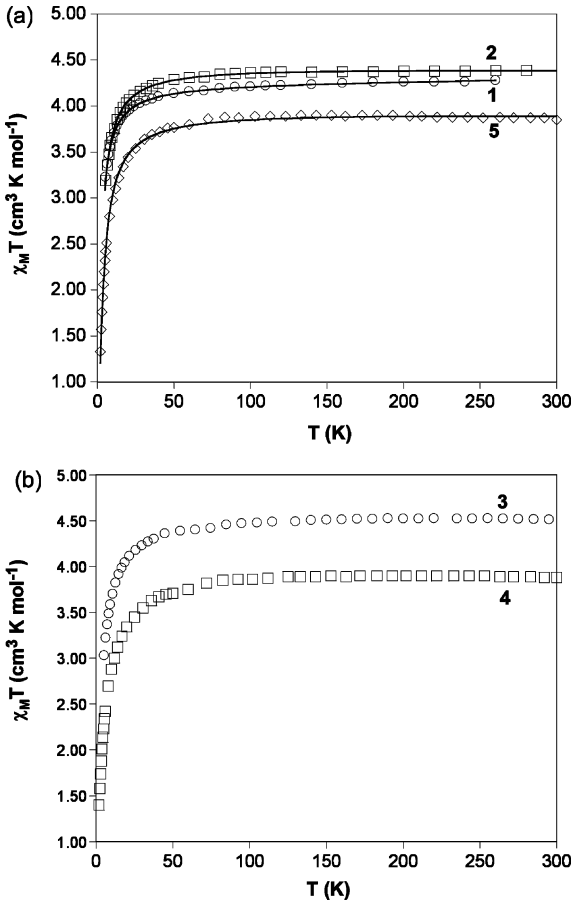

Figure 8. Thermal behavior of $\chi_M T$ at 5 kOe for (a) compounds **1** (○), **2** (□), and **5** (◇) and (b) **3** (○) and **4** (□). The $\chi_M T$ values for **1**−**4** were calculated on a per-Mn basis and those for **5** on the basis of a $Mn_{0.5}Fe_{0.5}$ content.

further proof of the efficiency of the pyrimidine-based ligands for the formation of highly accessible porous networks. In this regard, the dianionic nature of the pmdc ligand results

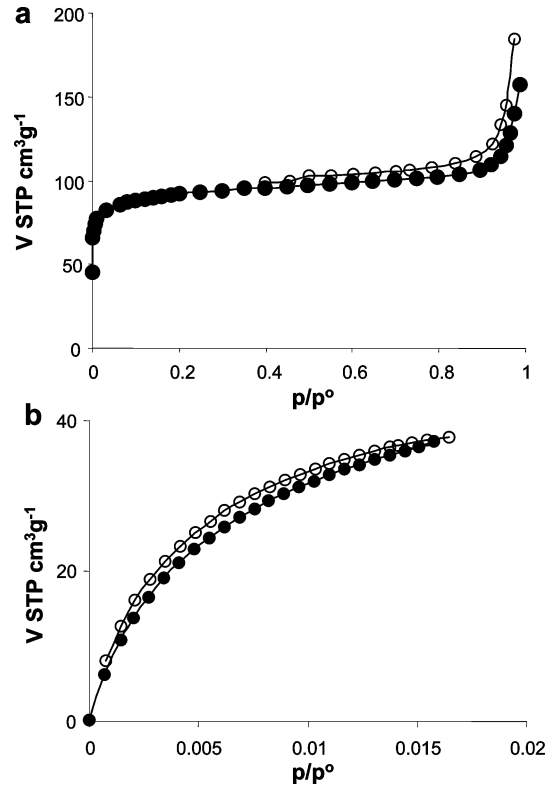

Figure 9. (a) N_2 adsorption isotherm of **4** at 77 K. (b) CO_2 adsorption isotherm of **4** at 293 K. Symbols: (●) adsorption, (○) desorption.

in a metal ion/organic ligand ratio greater than that previously reported for $[M(pyrimidinolate)_2]_n$ materials.[13,35] The presence of a larger number of metal ions in the network may result in greater accessibility of the polarizing metal centers, resulting in a stronger adsorbate−adsorbent interaction.[36]

Conclusions

The anionic nature of the pmdc ligand leads to the formation of neutral and, in the case of **4**, thermally robust networks. Variation of the synthetic conditions coupled with the plasticity of Mn(II) leads to a wide diversity of structural,

(35) Navarro, J. A. R.; Barea, E.; Salas, J. M.; Romero, M. A.; Quirós, M.; Masciocchi, N.; Galli, S.; Sironi, A.; Lippert, B. *J. Solid State Chem.* **2005**, *178*, 2436.
(36) (a) Chen, B.; Ockwig, N. W.; Millward, A. R.; Contreras, D. S.; Yaghi, O. M. *Angew. Chem., Int. Ed.* **2005**, *44*, 4745. (b) Dinca, M.; Yu, A. F.; Long, J. R. *J. Am. Chem. Soc.* **2006**, *128*, 8904.

magnetic, and adsorptive properties, with examples of 1D, 2D, and even microporous 3D species. The crystal-to-crystal interconversion pathways among these species, which are favored by temperature and humidity changes, have been studied using a combination of conventional single-crystal techniques and powder diffraction methods. Studies of the sorptive properties of **4** with respect to environmentally relevant gases other than N_2 and CO_2 and the extension of this kind of reaction to other transition-metal ions are anticipated.

Acknowledgment. This work was supported by the Spanish Ministerio de Educación y Ciencia (MAT2005-03047, CTQ2005-00329/BQU, SB-2005-0115, and HI2006-0116) and by the Italian Ministero dell'Università e della Ricerca (PRIN 2006: "Materiali ibridi metallo-organici multifunzionali con leganti poliazotati"). Finantial support by Fondazione Cariplo is also acknowledged. G.B. thanks the Eusko Jaurlaritza/Gobierno Vasco for a doctoral fellowship (BF102.79). W.-g.W. thanks the Spanish Ministerio de Educación y Ciencia for a postdoctoral fellowship. G.T. thanks the Italian Ministero dell'Università e della Ricerca for a doctoral grant (Progetto Giovani 2006). The authors are also grateful to Prof. N. Masciocchi and Prof. M. A. Romero for helpful discussions.

Supporting Information Available: Hydrogen-bonding parameters for compounds **1**−**3** and **5**, thermal analysis (TG, DTA, and/or DSC) curves for compounds **1**−**5**, and X-ray crystallographic files in CIF format. This material is available free of charge via the Internet at http://pubs.acs.org.

IC8002788